Chapter-5

Electrochemical Corrosion behavior of Ta-coated 316L Stainless Steel

5.0 Introduction

Surgical metal implants are a structural component specifically used to strengthen a bone. A group of implants comprises bolt and nut compression plates attached to the bone. This is particularly useful when traditional methods (excluding implants) could cause cartilage atrophy and body joining to be exclusively long **[156].** Austenitic stainless steel is widely used in osteosynthesis because of its outstanding mechanical properties, corrosion resistance and value for money. However, the formation of chlorides (Cl^-) at high levels along with the regular human body temperature could create localised corrosions such as pitting, cramping and fatigue of the cargo by using this type of stainless steel. Due to machining imperfections and crevices, formation occurs, resulting in fatigue crack formation **[157].** Surgical implants are typically made of metals such as cobalt-chromium alloys, austenitic stainless steel and titanium and its alloys. Austenitic stainless steels are the most used metallic materials because of their comparative ease of manufacturing, low cost, and good corrosion resistance.

On the other hand, Austenitic stainless steels are prone to localized corrosion **[158].** Metal ions with 316L stainless steel have been suggested to be toxic to estrogenic cells and affect their spread and differentiation. In specific concentrations, the usual behaviour of osteoblast-like cells can be disturbed by-products of stainless-steel corrosion; dental and surgical alloy biocompatibility is primarily associated with corrosion. The corrosion resistance of biocompatible alloys is significant for human body implants because it determines a device's life and because corrosion products in

living organisms are harmful. The cell metabolism of corrosion products was detected. This means that corrosion current may be impaired by cell behaviour **[159].** The body is not considered hospitable to an implanted metal alloy with a high pH of saline electrolyte of approximately 7.4 and a temperature of 98.6°F (37°C). While chloride solutions are well known to be among the most aggressive and corrosive to metals, the ionic composition and protein concentration of body fluids make the new understanding of biomedical corrosion even more difficult. Alloy composition variations can lead to subtle differences in mechanical, physical or electrochemical characteristics **[160].** Four main groups were divided into orthopedic implants: osteosynthesis (stabilization and bone fixation); joint substitutions; Unconventional modular tumor implants; spine implants **[161**]. While the human body's pH levels are generally maintained at 7.0 levels, the pH value changes from 3 to 9 for many reasons, including accidents, biological imbalances, chronic illness, infection, etc., and pH levels near implants typically vary from 5.3 to 5.6 post-surgery **[162].**

The implants include temporary implants, such as flats and screws and permanent implants used to substitute the hip, knee, spine, shoulder, toe, finger, etc. Cutting corrosion in shielded areas at the screw/plate interface and in the under heads of the fastening tors and pitting corrosion of the SS implants is the mechanism for corrosion in temporary implants. The leading cause is worn, which, in turn, accelerates corrosion. The deposition of resistant corrosion coating on their surfaces is one of the most popular and economical ways to improve corrosion resistance in metallic structures. Direct current magnetron sputtering deposition is one of the physical vapor deposition (PVD) techniques that have been quickly developed for industrial applications over the past few decades, including the production of tough, wear, low friction, corrosion-resistant and decorative filings and other thin-shaped systems with specific electrical and optical characteristics. Sputtering

is a cost-effective method, and a highly purified and homogeneous finish can be deposited in large areas with strong substrate adhesion. Characteristics of stainless-steel metallic implants are summarized in **Table 5.1.**

Table 5.1 Orthopaedic characteristics of stainless steel metallic implant **[156]** and **[163].**

Design-nation	Principal Alloying Element (wt.%)	Primary Utilizations	Advantages	Disadvantages
F-138 ASTM	Ni (12-14), Mo (2-4), Cr (17-20), and Fe (Bal.)	Temporary devices (hip nail, screw, fracture plates) used for THRs stem in the UK (Rich N2), joint arthroplasty, and osteosynthesis.	Availability processing, cost, fatigue resistance, corrosion resistance, high wear resistance	High modulus with long-term behaviour, high friction coefficient, ascetic loosing, generation of wear debris

In this study, stainless steel type 316L is coated with tantalum (Ta) with a thickness of 1.504µm, 3.893 µm, and 6.083µm duration of 15, 30, and 60 minutes, respectively, by using a DC magnetron sputtering system. Then, metallurgical characterization was done by Optical Microscopy (OM), Scanning Electron Microscopy, Energy Dispersive X-ray Spectroscopy, and X-ray photoelectron spectroscopy (XPS) for both Ta-coated and bare 316L SS after investigating electrochemical corrosion behaviour. In order to use the long-term applications without internal implant failure and effective performance (especially Ta-coated 316L SS) to the orthopedic applications.

5.1 Experimental Procedure

5.1.1 Materials and Sample Preparation

Austenitic stainless steel 316 L was received from Mishra Dhatu Nigam Limited (MIDHANI), Hyderabad, India. The Stainless-steel type 316L had dimensions of 472 × 775 × 20mm. The typical chemical compositions as received are given in **Table 5.2.**

Table 5.2 The chemical composition of 316L stainless steel in wt.%

Material	Cr	Ni	Mo	Mn	C	S	P	Si	Fe
316L SS	17.5	13.6	2.27	1.39	0.03	0.005	0.003	0.015	Balanced

The required number of samples (four in this case) of dimensions 20×20×2 mm were prepared from the received sample of 316L SS with the help of a table-moving CNC wire-cut EDM machine. Samples were mirror-polished before the deposition of the Ta coating using emery paper up to 1600 grit, followed by washing with distilled water and blow drying with hot air. The specimens were then ultrasonically cleaned with acetone for 10 minutes to achieve good adhesion with the coating. Optical microscopy was used to check the substrate constantly to ensure the microstructure of the sample surface.

5.1.2 Deposition of tantalum

Direct current magnetron sputtering (DCMS) is a thin film of physical vapor deposition (PVD); the coating process in which the target material to be coated is bombarded with ionized gas molecules causes atoms to be “sputtered” off into the plasma. These vaporized atoms are subsequently deposited as a thin film on the substrate to be coated when they condense.

Fig. 5.1 shows the systematic DCMS process. The thin film was deposited with high purity sputter tantalum target (99.95% Ta) with a dimension of 55.8mm diameter and 3.175 mm thickness onto stainless steel 316L (20 × 20 mm^2) by the DCMS. Constant argon (Ar) gas flows with a current rate of 0.15 amp was used as the optimal deposition condition. The chiller temperature was maintained at 20˚C and a voltage range of 270-276V. Magnetron source shutters were provided for pre-ionizing. Special magnetics fulfil the requirement of uniformly sputtering. To accommodate a single target, argon gas flow was uniformly distributed inside the chamber for the thin film preparation of tantalum. Tantalum was deposited on 316L SS specimens (3 nos.) for 15 minutes, 30 minutes and 60 minutes by DCMS to achieve a certain level of variation in thickness. For all the proceedings, the subtract holder's distance to the target was kept at 70mm, its rotation speed at 7-9 rpm and its working temperature at 180˚C. The chamber's base pressure and working pressure were maintained below $5x10^{-4}$ Pa and $5x10^{-1}$ Pa, respectively. The proportion of argon gas with a flow rate of 16 sccm and deposition pressure was controlled by a mass flow controller (MFC).

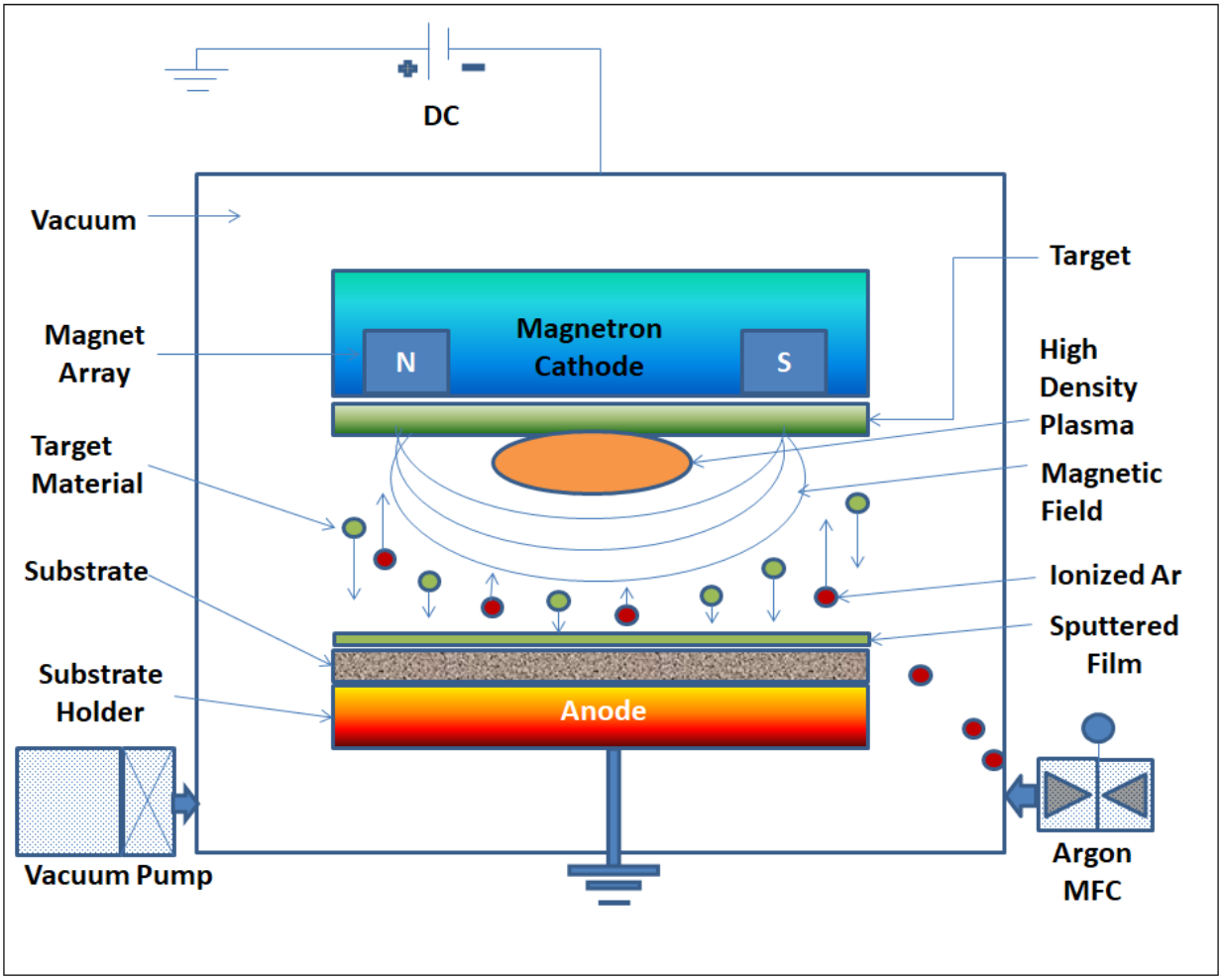

Fig. 5.1 Systematic direct current magnetron sputtering (DCMS) process

5.1.3 Microstructure analysis

Before the Ta coating was observed, all three specimens 316L SS surface used an optical microscope (OM, LeicaZ6 APO) and were investigated by the energy dispersive X-ray spectrometry (51N1000 – EDS System, Oxford Instruments Nanoanalysis) and Scanning Electron Microscopy (SEM, ZEISS MA 15/18, UK) and after the coating also it was characterized. The sample was then coated with tantalum for 15, 30, and 60 minutes by the DC sputtering machine; the 316L SS was examined to observe surface morphology by scanning electron microscopy

(SEM), and the chemical composition of the samples was determined by energy dispersive X-ray spectrometry (EDS). X-ray Photoelectron Spectroscopy (K-alpha, Thermo Fisher Scientific) was used to identify the chemical states and elemental composition of the Ta-coated and bare 316L SS. The surface nano analysis XPS system used a 150W non-monochromatic Al Kα radiation of 1486.6 eV. The XPS survey and core spectra of Ta, Fe, O, Cr, Mo, Ni, Mn, and C were determined.

5.1.4 Electrochemical Corrosion Analysis

Electrochemical measurement was characterized by potentiodynamic polarisation and an electrochemical impedance spectroscopy (EIS) test. The samples were tested in simulated body fluid (SBF) and prepared using the high-purity chemicals in **Table 5.3**. The typical three-electrode system, in which 316L SS act as a working electrode, platinum electrode (Pt) acts as an auxiliary electrode and silver chloride electrode (Ag/Ag Cl) acts as a reference electrode, was used for the electrochemical corrosion measurement.

Table 5.3 Composition of simulated body fluid at 7.4pH **[164]**

Constituents	NaCl (gram)	$NaHCO_3$ (gram)	KCl (gram)	$(CH_2OH)_3CNH_3$ (gram)	$MgCl_2.6H_2O$ (gram)	1.0 HCl (ml)	$CaCl_2$ (gram)	Na_2SO_4 (gram)
Amount in 1000 ml	8.035	0.355	0.225	6.118	0.10	39	0.292	0.072

5.2 Results and Discussion

5.2.1 Characterization of Bare 316L SS

The energy dispersive X-ray analysis of the bare 316 L samples indicates a high content of Cr, Ni, Mn, Fe, etc., as the components of 316L SS shown in **Fig. 5.2** of the EDX images. The SEM micrographs of the 316L SS bare sample in Fig. 5.3 showed no surface irregularities at 100X magnification. Before tantalum coating and corrosion studies, it is essential to ensure no defects are present on the surface.

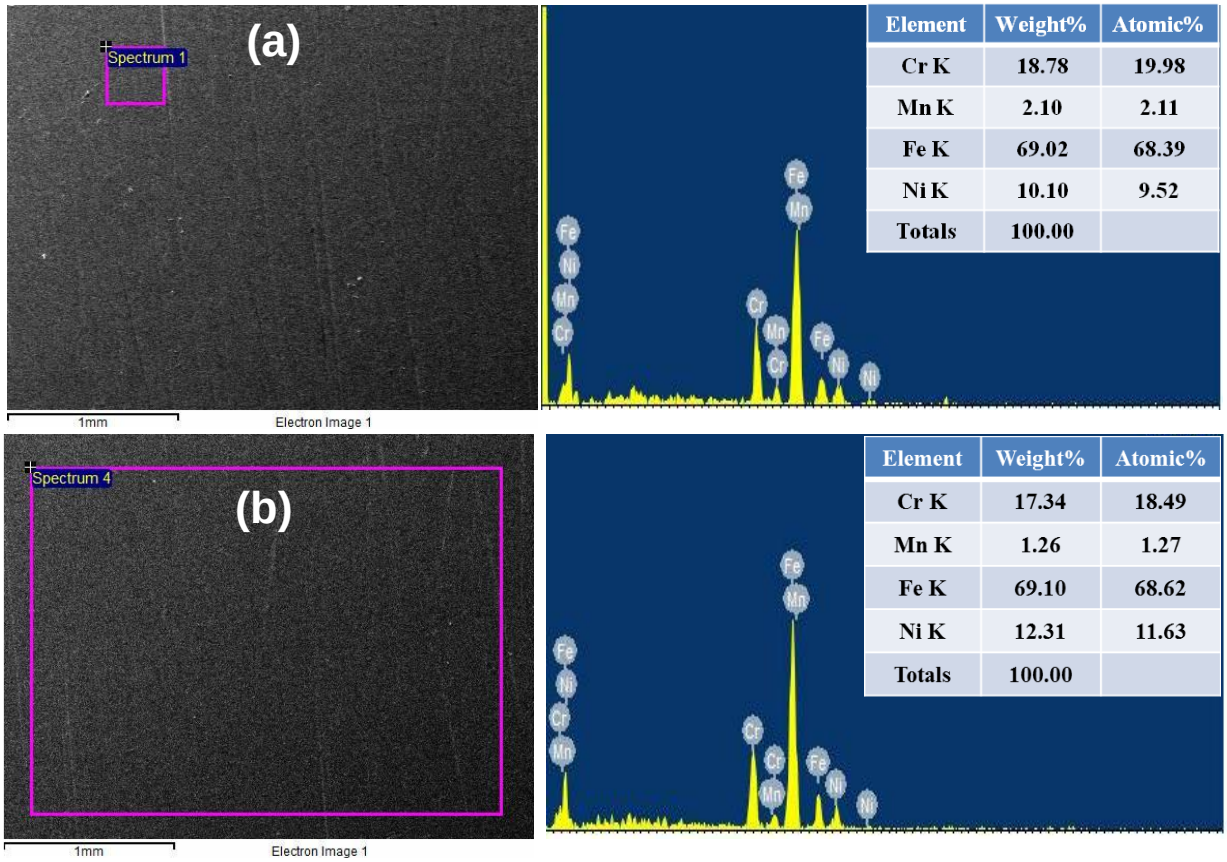

Fig. 5.2 EDX images of bare samples (a) EDX image of bare 316L SS at spectrum-1 (b) EDX image of bare 316L SS at spectrum-4

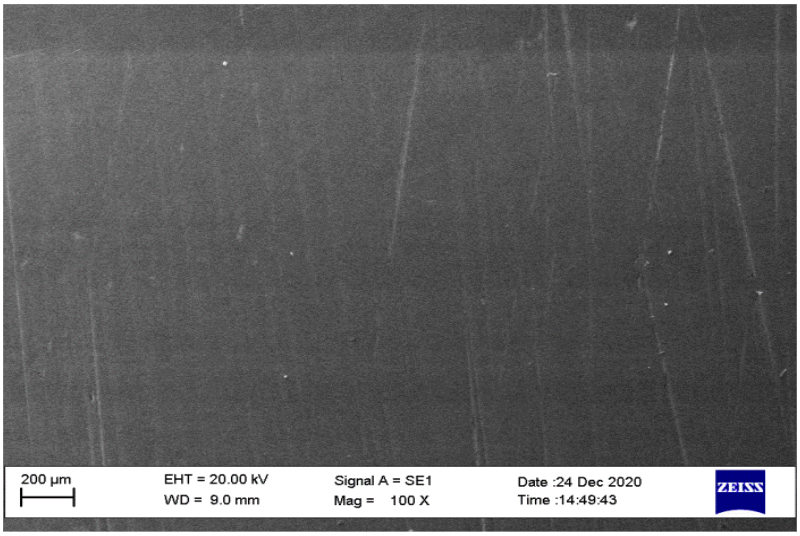

Fig. 5.3 SEM image of bare 316L SS

5.2.2 Characterization of Ta-Coated 316L SS

The energy-dispersive X-ray analyses of the Ta-coated 316 L samples were carried out for all three samples. It was observed that only Ta was present, which confirms the uniform coating of Ta on the surface of 316L SS as shown in **Fig. 5.4**. Further Ta-coated 316L SS samples were examined using SEM to determine surface morphology which is essential to assess before corrosion studies. **Fig. 5.5** is the SEM images of Ta-coated 316L SS from 15 to 60 min before corrosion. The results in **Fig. 5.5b** (3.893 µm) suggest that the average coating thickness is 3.699±0.194 µm. The same micrographs were used to determine the thickness of the Ta coating. SEM confirmed the absence of any significant pits. The coating thicknesses for the three samples are listed in **Table 5.4.** The thickness was uniform and increased with the increase of the coating deposition time. The minimum thickness was 1.504 µm for 15 minutes of deposition, and the maximum was 6.083 µm for 60 minutes. All the SEM micrographs are presented in **Fig. 5.5** for 200X and 400X magnifications.

Table 5.4 Ta-coated thickness by DC magnetron sputtering on 316L with time interval.

Sample	Coating Time (minutes)	Thickness of coating (μm)
316L SS	15	1.504±0.042
316L SS	30	3.699±0.194
316L SS	60	6.083±0.028

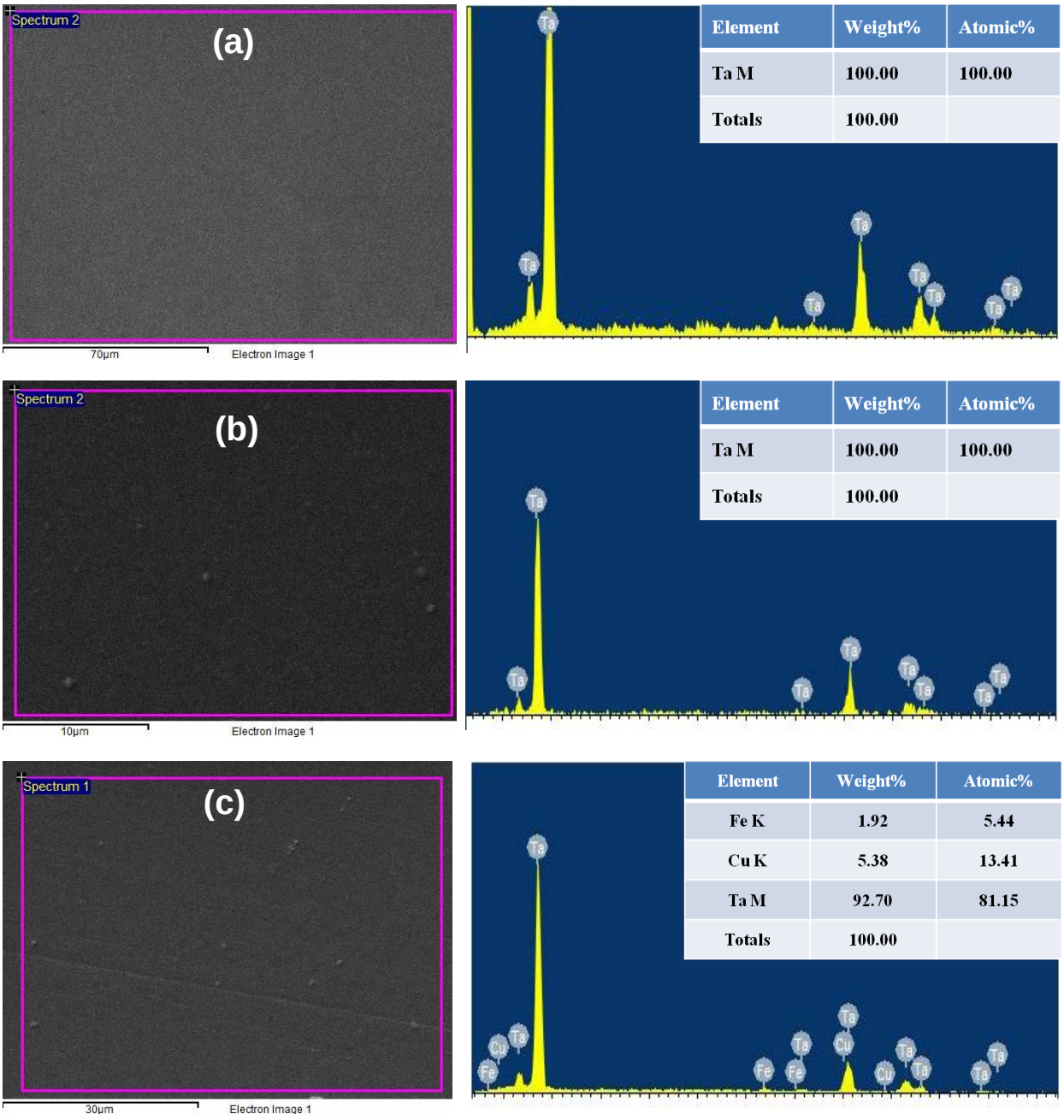

Fig. 5.4 EDX images of Ta-coated 316L SS samples (a) 15 min. (b) 30 min. (c) 60 min.

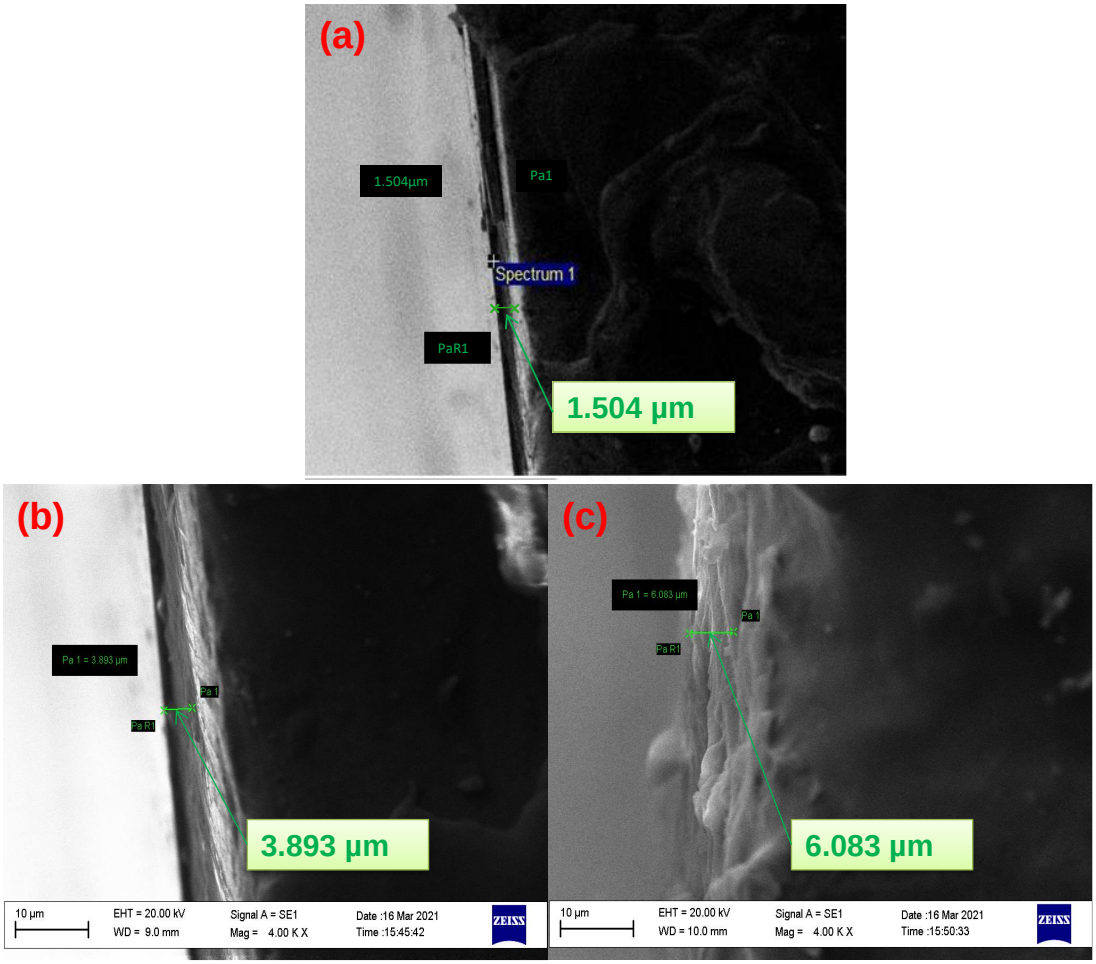

Fig. 5.5 SEM images before corrosion of Ta-coated 316L SS (a) 15 min. Ta-coating (b) 30 min. Ta-coating (c) 60 min. Ta- coating

As-sputtered multilayer Ta/Ta_2O_5 thin film had a shiny appearance, as illustrated in **Fig. 5.6** and appeared in exquisite black due to the effect of argon flow rate ratio and deposition power on surface morphology and cross-sectional microstructure. However, after the potentiodynamic polarization test, this original appearance faded to a bland white. Features of the as-sputtered and annealed Ta/Ta_2O_5, such as shape and compositions, were compared using SEM microstructural and elemental analyses. Fig. 6 shows the surface morphology of as-sputtered thin film samples with their cross-sectional microstructure under various magnetron-sputtering experimental

settings. Tantalum is an effective seed layer for Ta film over the 316L SS, producing a fine-grained structure with a smoother surface.

Furthermore, the tantalum system has a consistent surface shape, as seen in **Fig. 5.6**, While multiple cracks and discontinuities can be seen in the single-layer Ta film. This is typically what causes the metastable Ta to form at the interface. Tantalum is available in two distinct phases: an α -phase, which is a stable body-centred cubic structure (bcc) and a β-phase with a tetragonal metastable structure that can be transformed into a β-phase by thermal treatment at high temperatures (750-950°C)[**165-166**].

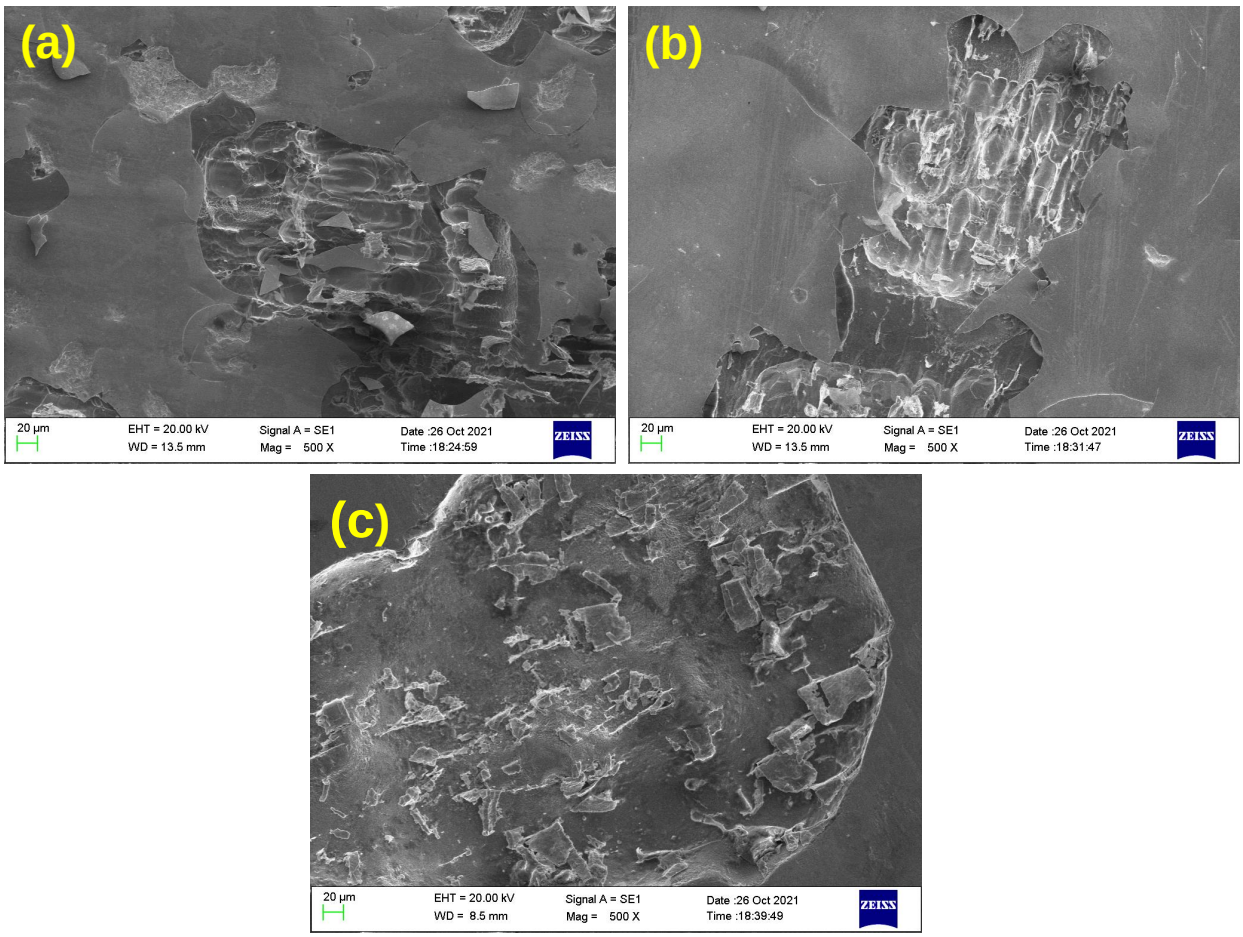

Fig. 5.6 SEM images after corrosion of Ta-coated 316L SS (a) 15 min. (b) 30 min. (c) 60 min.

5.2.3 X-ray Photoelectron Spectroscopy (XPS)

In **Fig. 5.7 (a–d),** the XPS broad scan survey spectra and core spectra for each element contained in the coating are plotted, and images are presented. In **Fig. 5.7**, the presence of characteristic peaks in relative binding energies of elements (Ta4f, C1s, N1s, O1s, Cr2p, Fe2p, Ni2p, and Mo3d) suggests that tantalum was successfully incorporated into the coating matrix. Before the corrosion test, the Ta4f core level of spectra located at binding energies from 2466.3 eV, 2337339.21 eV, and 4213045.02 eV, simultaneously 0.01%, 6.99%, and 12.27% atomic percentages achieved Ta coated stainless steel type 316L (15 min., 30 min., and 60 min.) respectively.

Notably, a pure Ta film's Ta4f spectrum has a significant shoulder at energy doublet, implying that the deposited film seems to be primarily metallic Ta. For bare 316L stainless steel, XPS spectra show the peaks of Ni, Fe, Cr, O, C, N, Mo, Al, and Ta coated for 15 min. sample represents the peaks of the Ni, Fe, Cr, O, C, Mo, and Ta, Ta coated for 30 min. The sample shows the peaks of the Ni, Cr, O, Ca, C, Mo, and Ta, Ta coated for 60 min. The sample shows the peaks of Ni, Cr, O, C, Mo, and Ta.

In **Fig. 5.8**, the XPS results of Chromium (Cr 2p), Aluminium (Al 2p), Molybdenum (Mo 3d), Nickel (Ni 2p), oxygen (O1s), carbon (C1s), Iron (Fe 2p), and Nitrogen (N 1s) spectra of bare stainless steel type 316L are presented. XPS spectra of 316L Stainless steel show which prominent peaks O, C, Fe, Ni, and Mo are present. The findings show that the examined surface layer contains chromium metal and compounds. Clear peaks of Molybdenum, nickel, carbon, and iron can also be seen.

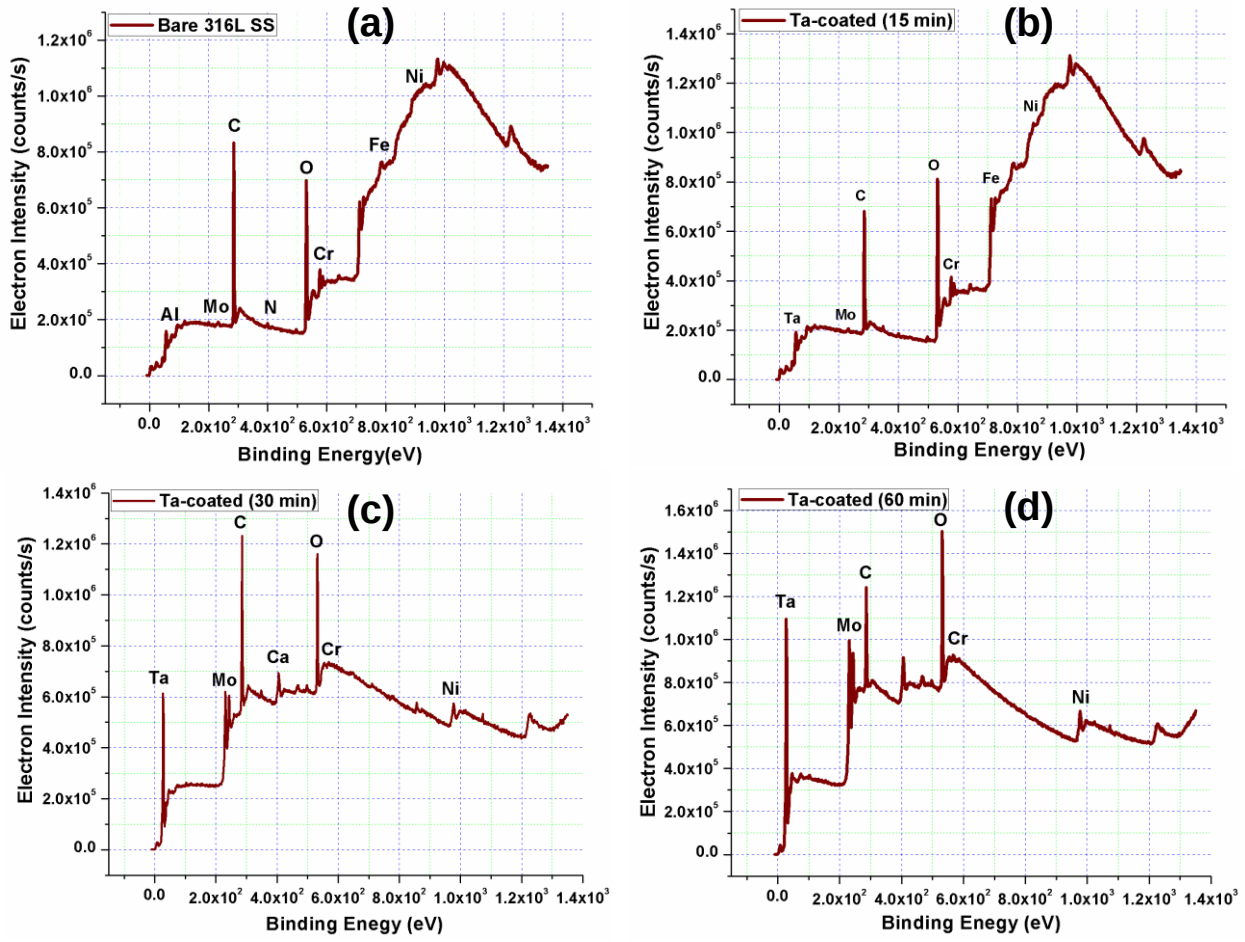

Fig. 5.7 XPS spectra of 316L Stainless steel (a) Bare (b) 15min. Ta-coated (c) 30min.Ta-coated (d) 60min.Ta-coated

Apart from oxides and hydroxides, the final one, with a lot of oxygen in the passive layer, can generate iron, chromium sulfide, and phosphates. Cr 2p and Fe2p fit better in understanding the chemical composition of the surface layer, as shown in **Fig. 5.8.** According to our findings, the change in chemical composition on the uppermost surface is closely related to corrosion resistance. After coating, the quantity of Cr in unoxidized stainless steel susceptible to corrosion is drastically reduced. It's essential to compare the Fe and O composition changes linked to product corrosion after coating. **Table 5.5** shows the compounds and binding energy (BE) of bare and coated 316L

stainless steel. These findings suggest that the initial amount of Cr, largely present in Cr_2O_3 before coating, significantly impacts corrosion resistance.

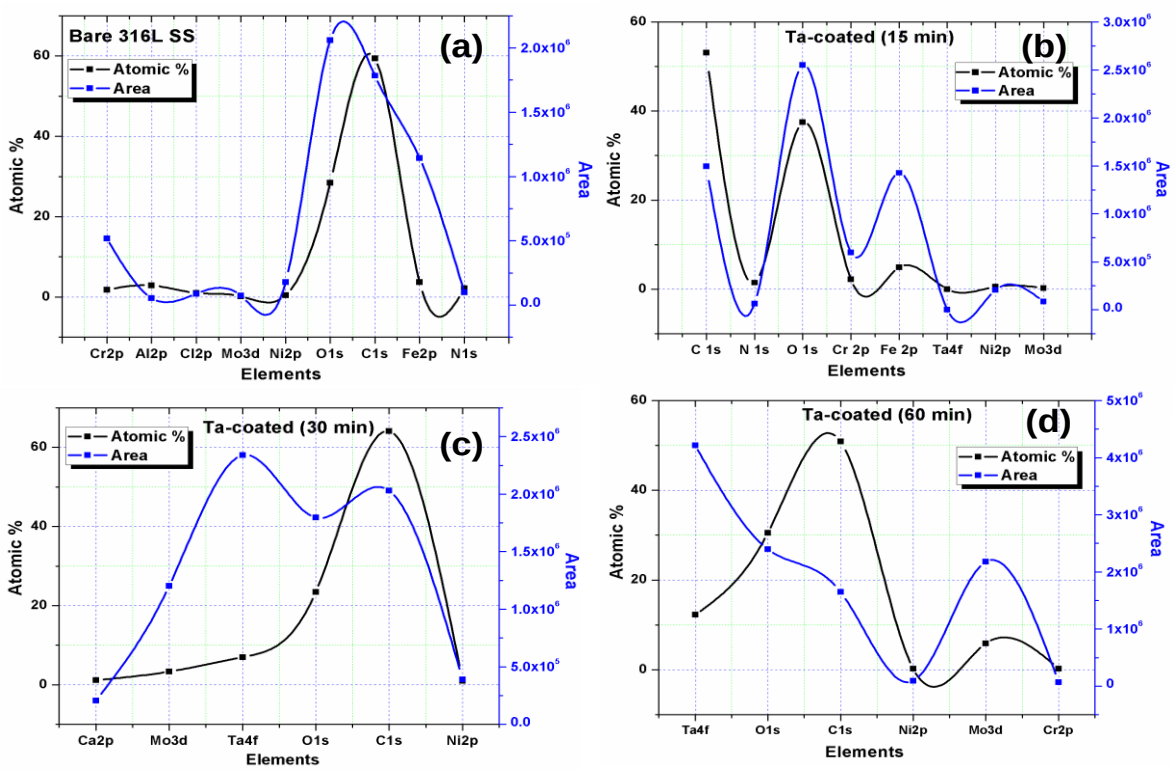

Fig. 5.8 XPS spectra (elemental and atomic %) of 316L Stainless steel (a) Bare (b) 15min. Ta-coated (c) 30min.Ta-coated (d) 60min.Ta-coated

Table 5.5 Compounds and Binding Energy (BE) of bare and coated 316L stainless steel

Bare 316l SS		Ta coated (15 min)		Ta coated (30 min)		Ta coated (60 min)	
Compounds (eV)	BE	Compo-unds	BE	Compounds	BE	Compounds	BE
Cr2p	594.08	C 1s	298	Ca2p	360.08	Ta4f	32.08
Al2p	76.58	N 1s	410	Mo3d	238	O1s	537.58
Cl2p	210.08	O 1s	540.45	Ta4f	32.58	C1s	298.08
Mo3d	238	Cr 2p	594	O1s	541.08	Ni2p	882
Ni2p	882	Fe 2p	735.54	C1s	298.08	Mo3d	238
O1s	538.08	Ta4f	28	Ni2p	882.08	Cr2p	592
C1s	294.58	Ni2p	882	-	-	-	-
Fe2p	737.08	Mo3d	238	-	-	-	-
N1s	410.08	-	-	-	-	-	-

5.3 Electrochemical Corrosion Analysis

5.3.1 Open Circuit Potential Study:

An open circuit potential (OCP) measurement was performed for 1 hour to ensure that the specimen's working surface was stable, and monitoring of 316L SS bare and Ta-coated 316L SS in simulated body fluid at pH of 7.4 and temperature of 37°C was completed. The potential was established between the working electrode and the environment with a reference electrode.

5.3.2 Electrochemical Impedance Spectroscopy Study:

An EIS test was performed by frequency sweeping the range from the initial 1000 Hz to the final 10 Hz at 0.2V potential against OCP at a scan rate of 10mV/Minute for 60 minutes logarithmic and 100 points in SBF at 37°C for all the samples (316L SS bare, and Ta-coated 316L SS from 15 to 60 Minutes), respectively. To obtain the corrosion rate and corrosion resistance data, the EIS tests were analysed with CView (CS studio, version 5.2) and ZView (CS studio, version 5.2) software. **Fig. 5.9** shows the experimental data of the equivalent electric circuit of bare and tantalum coating samples. The proposed model contains three time constraints: the solution resistance (RS), constant phase element-1 (CPE-1) connected in series, constant phase element-2 (CPE-2) connected in parallel along with resistance (R) of the electrolyte and Warburg impedance (W). Furthermore, at the base of micropores, the bare and coated samples arranged in parallel capacity could be assumed to be equal so that only a single element is used **[167].** The constant phase element (CPE) can be used to simulate the non-ideal behaviour of a capacitor [**168].** It could be defined by two values: CPE-T (T) and CPE (P). The CPE is defined as equ.1:

$$Z = 1/ [T_{(jw)}{}^{n}] \quad (1)$$

Where $j=\sqrt{-1}$, $w= 2\pi f$ is an angular frequency (rad/s), and f is the frequency (Hz), n is known as a dimensionless number related to non-uniform current distribution because of the surface inhomogeneity and roughness, which varies between 0.75 and 1.

The anodic oxidation of tantalum coating in an anodic solution leads to the formation of Ta_2O_5 [**169-170].** The corresponding cathodic half-reaction is as follows equ.2 [**171**]**:**

$$Ta_2O_5 + 10H^+ + 10e^- \leftrightarrow 2Ta + 5H_2O \quad [E = 0.75 \text{ vs. SHE}] (2)$$

Fig. 5.9 for the equivalent electric circuit demonstrates the bare and coated samples, in which R_s represents the solution resistance, CPE_1 and R_1 represent capacitance and resistance of the porous product layer of corrosion, and CPE_2 and R_2 belong to the capacitance and resistance of electrical double layer between alloys interface and product of the corrosion. **Table 5.6** shows the parameters of the equivalent electrical circuit (EEC) model bare and coated samples in 7.4 pH. The EEC is used to explain whether a process operates when there are two time constants: a high-frequency (HF) time constant (CPE_1-R_1) and a low-frequency (LF) time constant (CPE_2-R_2).

Fig. 5.10 depicts the Nyquist plot for bare and Ta-coated 316L SS in SBF at 7.4 pH. The EEC parameter values were calculated using the experimental data. The HF time constant's physical meaning is to speed up charging/discharging and charge transfer operations, represented by a parallel combination of the double layer/space charge capacitance (CPE_1) and the charge transfer resistance (R_1). The LF time constant (CPE_2-R_2), on the other hand, is associated with slower mass transport phenomena in the oxide phase, such as electroactive ions migration through the use of the generated passivity. **Figure 5.11** shows the Bode plot for bare and Ta-coated 316L SS in SBF at 7.4 pH.

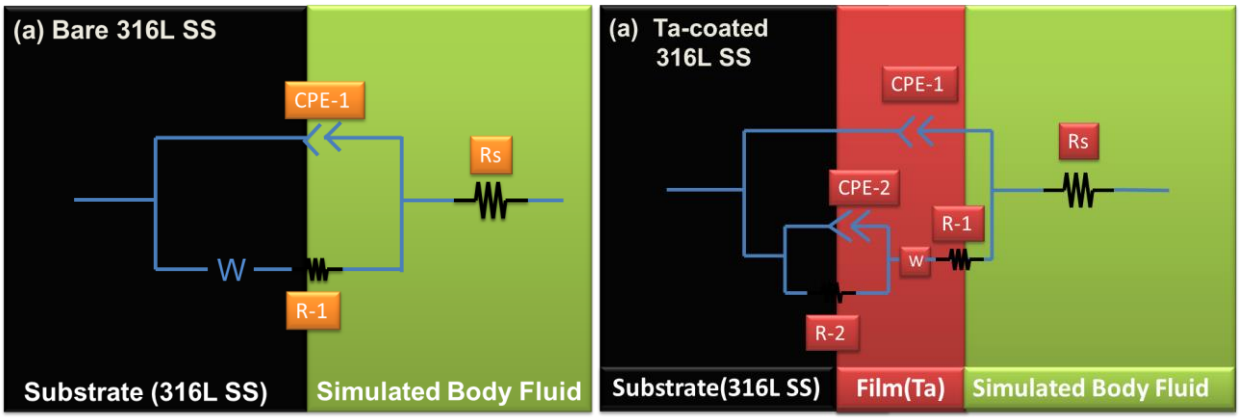

***R_s = Solution Resistance, CPE = Constant Phase Element, R_1= Resistance of Porous product layer of corrosion, R_2= Resistance of alloy interface & product of corrosion, and W = Warburg Impedance**

Fig. 5.9 Equivalent electric circuit (EEC) for a) 316L SS (bare) and b) Ta-coated-316L SS

Table 5.6 Parameters of the equivalent electrical circuit model bare and coated samples in 7.4 pH

Samples	R_s Ωcm^2	R_1 Ωcm^2	CPE_1		R_2 Ωcm^2	CPE_2		R_w Ωcm^2	$\chi^2 * 10^{-4}$
			Y_1*10^{-6} $\Omega cm^{-2}s^n$	n_1		Y_2*10^{-9} $\Omega cm^{-2}s^n$	n_2		
316L BARE	73.22	1878	0.85	0.75	-	-	-	6123	0.2496
Ta-Coating (15Min.)	89.76	3864	0.40	0.81	10170	1.57	0.76	25.94	0.2412
Ta-Coating (30Min.)	90.40	40931	3.82	0.85	20.58	1.94	0.86	18965	0.2641
Ta-Coating (60Min.)	80.80	61291	1.63	0.77	46418	0.72	0.79	23990	0.2818

The Nyquist plot for Ta-coated 316L SS may also show a semicircle, but its characteristics will depend on the different thicknesses of the tantalum (Ta) coating. The Ta coating (60min.) is effective, and the semicircle diameter was found to be much larger compared to the 15 and 30min. Ta-coated 316L SS, indicating an improvement in corrosion resistance shown in **Fig. 5.10.**

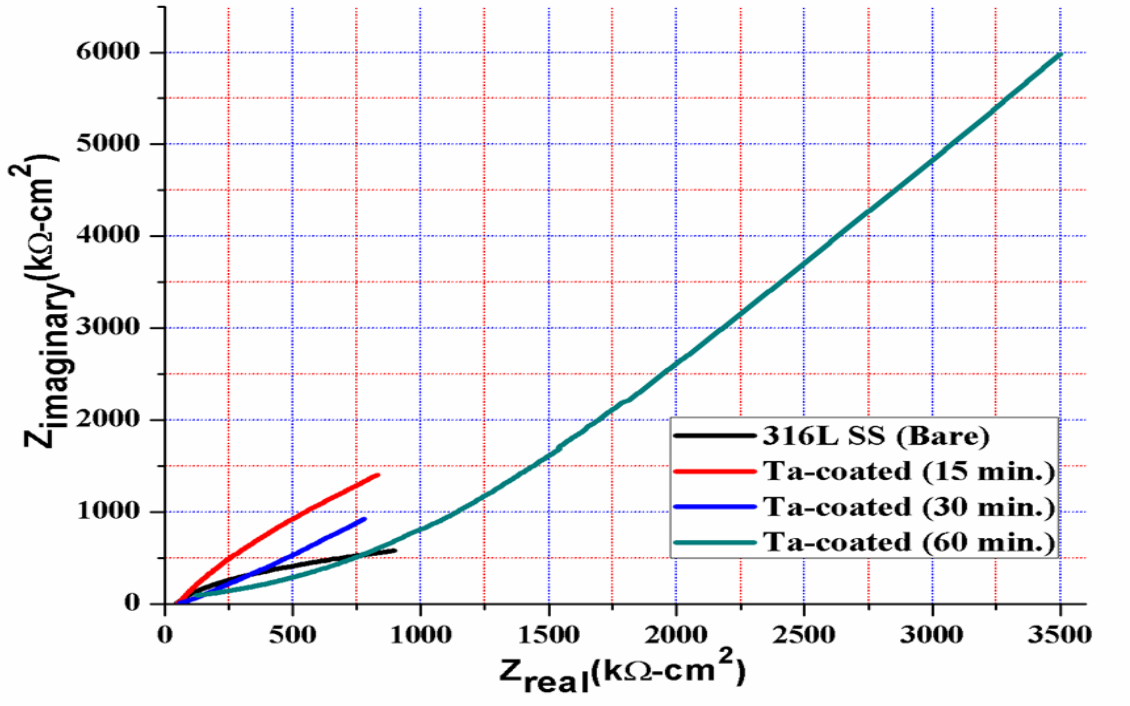

Fig. 5.10 Nyquist plot for bare and Ta-coated 316L SS in SBF at 7.4 pH

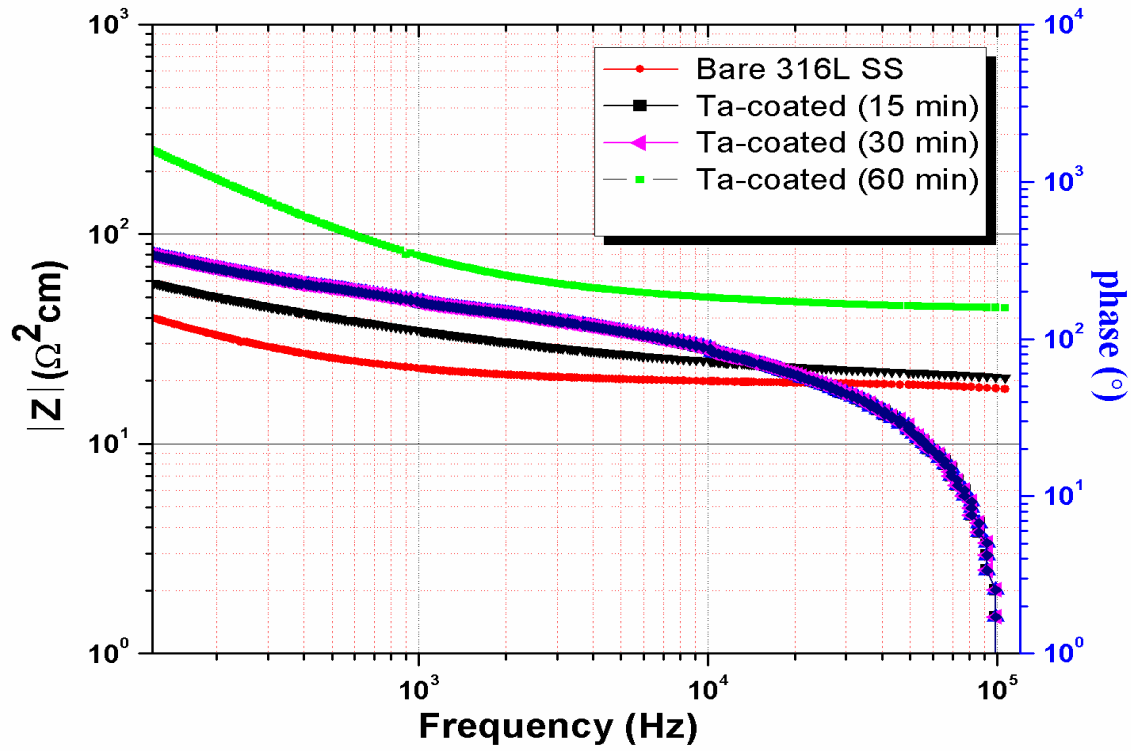

Fig. 5.11 Bode plot for bare and Ta-coated 316L SS in SBF at 7.4 pH

5.3.3 Potentiodynamic Study

Tafel's extrapolation of the relevant polarisation parameters revealed polarisation curves for the bare and Ta-coated 316L stainless steels shown in **Fig. 5.12.** It has been observed that I_{corr} decreases with an increase in coating thickness, indicating that the corrosion product also acts as protection from further corrosion. The E_{corr} for 316L SS was greater in the coated sample than in the bare sample. This indicates that the spontaneity of corrosion is less for the coated sample than that of bare samples. It was observed that 316LSS has minimum breakdown potential among all other samples. Corrosion parameters and performance of all the samples are given in **Table 5.7** at a pH of 7.4 and 37^{o}C. The potentiodynamic polarization curve was obtained according to DOE specifications for anodic corrosion [**172-183],** shown in **Fig. 5.12.** As a result, it has been established that the corrosion protection provided by this Ta-based coating increases with time from 15 minutes up to 60 minutes. It should also be noted that the Bode diagram's high-frequency region contains data about coating flaws and changes in surface area**.** To verify the stability of passivation film at a given voltage range of about 3V, because the change in corrosion potential is dependent on a change in one or both of the anodic and cathodic reactions, the long-term change in corrosion potential (open-circuit potential) represents a change in a corrosion system. For example, an increase in corrosion potential might be attributable to a decrease in the anodic reaction due to forming a passive layer. A sharp increase in current density is located when a potential is reached at 2.7693E-1, signalling the passivation film breakdown after the constant potential from 6.8407E-2 to 9.2607E-4. An empirical equation to evaluate the porosity (P) of the coatings and protective efficiency is **[173-197];**

$$\mathbf{P} = \frac{\mathbf{RpS\ (Subtract)}}{\mathbf{Rp\ (Coating/\ Subtract)}} \times \left(\nabla \boldsymbol{E}_{\frac{corr}{\beta}}\right) \quad \textbf{(3)}$$

Here, P is the total coating porosity, R_ps is the polarisation resistance of the substrate material, Rp is the calculated polarisation resistance of the coated system, ΔE_{corr} is the potential difference between the bare substrate steel and the corrosion potential of the coated steel and β is the anodic Tafel slope of the substrate **[174].**

The calculated polarisation resistance (Rp) of the coated system is:

$$\mathbf{Rp} = \frac{\boldsymbol{\beta a * \beta c}}{\{\mathbf{2.3x\ icorr\ x\ (\beta a+\beta c)}\}} \quad \textbf{(4)}$$

Here, βa is the anodic Tafel constant, and βc is the cathodic Tafel constant. The protective efficiency (Pi) of the coating is determined from the polarization curve by the following equation;

$$\mathbf{Pi} = \mathbf{100} * \frac{\mathbf{1-iCorr}}{\mathbf{i0Corr}} \quad \textbf{(5)}$$

Here, i_{corr} and i^0_{corr} are the corrosion current densities in the presence and absence of the coating, respectively.

Fig. 5.12 shows Tafel curves generated using the Tafel polarisation method after a 1 h holding period of coated and untreated AISI 316 L austenitic stainless steel in SBF medium. A lower corrosion current density signifies better corrosion resistance, indicating that the metal is less prone to corrosion. In contrast, higher corrosion current density implies lower corrosion resistance, indicating an increased susceptibility to corrosion. Because the Icorr values of the AISI 316 L austenitic steel were greater than the uncoated state and the Rp values were substantially lower

than the uncoated condition, the corrosion resistance of the Ta-coated samples in the SBF medium appears to be lower than expected.

Table 5.7 Polarization parameter for bare and Ta-coated 316L SS in 7.4pH at 37°C

Sample	βa (mv)	βc (mv)	I_0 (A/Cm^2) (×10^{-6})	E_o (V)	CR (mm/y)
316L SS (Bare)	586.52	484.99	25.043	-0.2375	0.2053
Ta-coated (15 min.)	270.69	255.13	5.519	-0.1171	0.0603
Ta-coated (30 min.)	1710.70	195.67	0.814	-0.2585	0.0196
Ta-coated (60 min.)	145.18	4164.90	0.197	-0.0034	0.0047

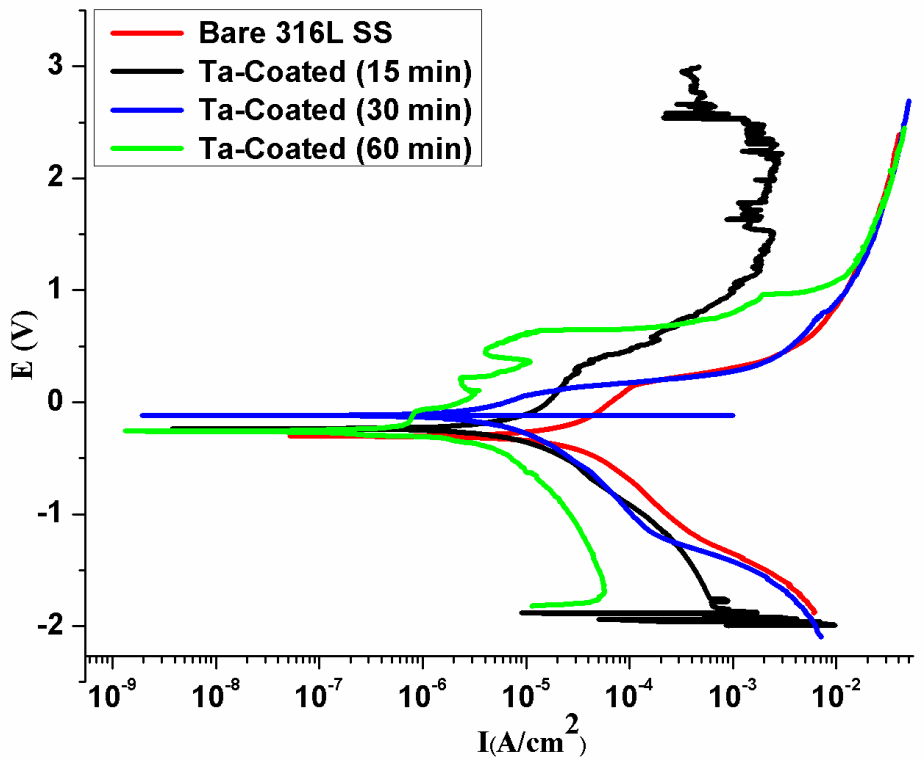

Fig. 5.12 Potentiodynamic polarization curve for bare and Ta-coated 316L SS

5.4 Conclusion

In this study, tantalum (Ta) coating was applied to 316L stainless steel (SS) using DC magnetron sputtering techniques, with deposition times of 15, 30, and 60 minutes, resulting in respective coating thicknesses of 1.504 µm, 3.699 µm, and 6.083 µm. Electrochemical corrosion measurements were conducted on both coated and bare samples in simulated body fluid at 37°C. The electrochemical impedance spectroscopy (EIS) revealed that the corrosion resistance of the coated samples primarily arises from the impedance offered by the corrosion product and the interface between the coating and the metal. In the potentiodynamic measurements, it was observed that the corrosion rate exhibits a descending trend with an increase in tantalum (Ta) thickness.

The highest corrosion rate, measured at 0.2053 mm/y, was recorded for bare 316L stainless steel, while the lowest rate, at 0.0047 mm/y, was achieved with a Ta coating applied for 60 minutes. Surface characterizations post-corrosion, conducted through scanning electron microscopy (SEM) and energy-dispersive X-ray spectroscopy (EDX), unveiled a stable coating interface between the Ta coating and substrate. To delve deeper into the chemical state and composition of the prepared Ta coatings and elucidate the source of their robust corrosion resistance against bare 316L SS, X-ray photoelectron spectroscopy (XPS) measurements were employed. The findings from XPS indicate that tantalum films on metal surfaces elevate corrosion potentials and reduce current densities, particularly passive current density, compared to 316L stainless steel. Consequently, the corrosion rate of Ta-coated 316L stainless steel is notably lower than that of its bare counterpart. This comprehensive analysis underscores the efficacy of Ta coatings in enhancing corrosion resistance on 316L SS surfaces.